APPLIED SCIENCES AND ENGINEERING

Powering rotary molecular motors with low-intensity near-infrared light

Lukas Pfeifer[1]*†, Nong V. Hoang[2]*, Maximilian Scherübl[1]‡, Maxim S. Pshenichnikov[2]§, Ben L. Feringa[1,2]§

Light-controlled artificial molecular machines hold tremendous potential to revolutionize molecular sciences as autonomous motion allows the design of smart materials and systems whose properties can respond, adapt, and be modified on command. One long-standing challenge toward future applicability has been the need to develop methods using low-energy, low-intensity, near-infrared light to power these nanomachines. Here, we describe a rotary molecular motor sensitized by a two-photon absorber, which efficiently operates under near-infrared light at intensities and wavelengths compatible with in vivo studies. Time-resolved spectroscopy was used to gain insight into the mechanism of energy transfer to the motor following initial two-photon excitation. Our results offer prospects toward in vitro and in vivo applications of artificial molecular motors.

INTRODUCTION

The ever-increasing synthetic possibilities open to chemists today are progressively enabling the rational design of molecular systems whose structures can perform controlled motion in response to external stimuli (*1*). In recent decades, this has made possible the genesis of the field of molecular machines straddling the frontier between chemistry and materials science (*2*–*7*). Synthetic motors and machines will allow the transition from static to dynamic systems introducing responsive function and movement to artificial materials reminiscent of the autonomous motion characterizing living organisms. Consequently, much effort has been devoted to the design and study of highly diverse structures, all of which have in common that, upon addition of energy, in the form of, e.g., light, electrical voltage, or chemical fuel, mechanical movement is performed (*1*–*7*).

Molecular motors are an important class of molecular machines that operate in a repetitive and progressive manner, unlike the more commonly used molecular switches. Therefore, any work carried out by a motor during one step is not undone by subsequent steps, allowing them to continuously drive systems away from equilibrium. One prominent concept of molecular motors is based on the unidirectional rotatory displacement of one part of a molecule relative to another around a central overcrowded alkene axle (*8*). During motor operation, photochemical *E*/*Z* isomerization and thermal helix inversion (THI) steps are performed in an alternating fashion (*9*). In these "power-stroke" motors, light adds energy to the system by populating a metastable (excited state) isomer, and this energy is dissipated in the thermal isomerization, leading to the formation of another stable (ground state) isomer (*4*). A high stability difference, ΔG, between the metastable and stable isomers in combination with the intrinsic chirality ensures the unidirectionality of the rotation (*10*, *11*). In recent years, conceptual studies have demonstrated the potential of artificial rotary molecular motors for the construction of functionalized soft materials (*12*–*15*) including an artificial muscle (*14*), responsive surfaces (*16*), and metal-organic frameworks (*17*). Their motion has, furthermore, been demonstrated to disrupt cellular membranes (*18*) and direct the fate of stem cells (*19*).

To realize the full potential of molecular motors as building blocks for the construction of functional molecular systems as well as in vivo applications, overcoming the need for high-energy ultraviolet (UV) light to drive the *E*/*Z* isomerization to initiate their rotation has been identified as a key challenge. This is due to the fact that near-infrared (NIR) light benefits from an increased penetration depth in human tissue and fewer potential photochemical side reactions. Recent approaches toward the development of visible light–powered artificial rotary molecular motors include complexation with metal cations (*20*), incorporation of extended π-systems (*21*), introduction of electronic push-pull regimes across the central alkene axle (*22*), and the construction of oxindole-derived motors (*23*). Hemithioindigo-derived molecular motors responsive to visible light have been described by Dube and colleagues (*24*, *25*). It has also been demonstrated that triplet-triplet energy transfer from an attached visible light–sensitive porphyrin dye can be used as an alternative means of excitation albeit only under strictly anaerobic conditions (*26*), strongly limiting the applicability of this approach. Direct two-photon absorption (2PA) of chemically unmodified artificial molecular motors by NIR light (*27*) revealed that extremely high light intensities (approximately TW/cm^2) are required to trigger motors' functionality due to their low 2PA cross section. This presents a severe limitation, as such intensities are close to the threshold for photodamage in cells and underlying tissue (*28*).

Here, we present a different concept: a motor that is efficiently powered by NIR light via resonance energy transfer (RET) from a covalently attached 2PA sensitizer (Fig. 1A), spatially separating the two functions of 2PA and rotation. This strategy also allows our system to remain functional at very low concentrations and in the presence of additional chromophores, enabling compatibility of this approach with biological environments. To gain further insight into the motor function, the energy transfer mechanism and excited-state

[1]Stratingh Institute for Chemistry, University of Groningen, Nijenborgh 4, 9747 AG Groningen, Netherlands. [2]Zernike Institute for Advanced Materials, University of Groningen, Nijenborgh 4, 9747 AG Groningen, Netherlands.
*These authors contributed equally to this work.
†Present address: Laboratory of Photonics and Interfaces, Department of Chemistry and Chemical Engineering, École Polytechnique Fédérale de Lausanne, 1015 Lausanne, Switzerland.
‡Present address: Organisch-Chemisches Institut, Westfälische Wilhelms-Universität, Corrensstrasse 40, Room I 333, 48149 Münster, Germany.
§Corresponding author. Email: m.s.pchenitchnikov@rug.nl (M.S.P.); b.l.feringa@rug.nl (B.L.F.)

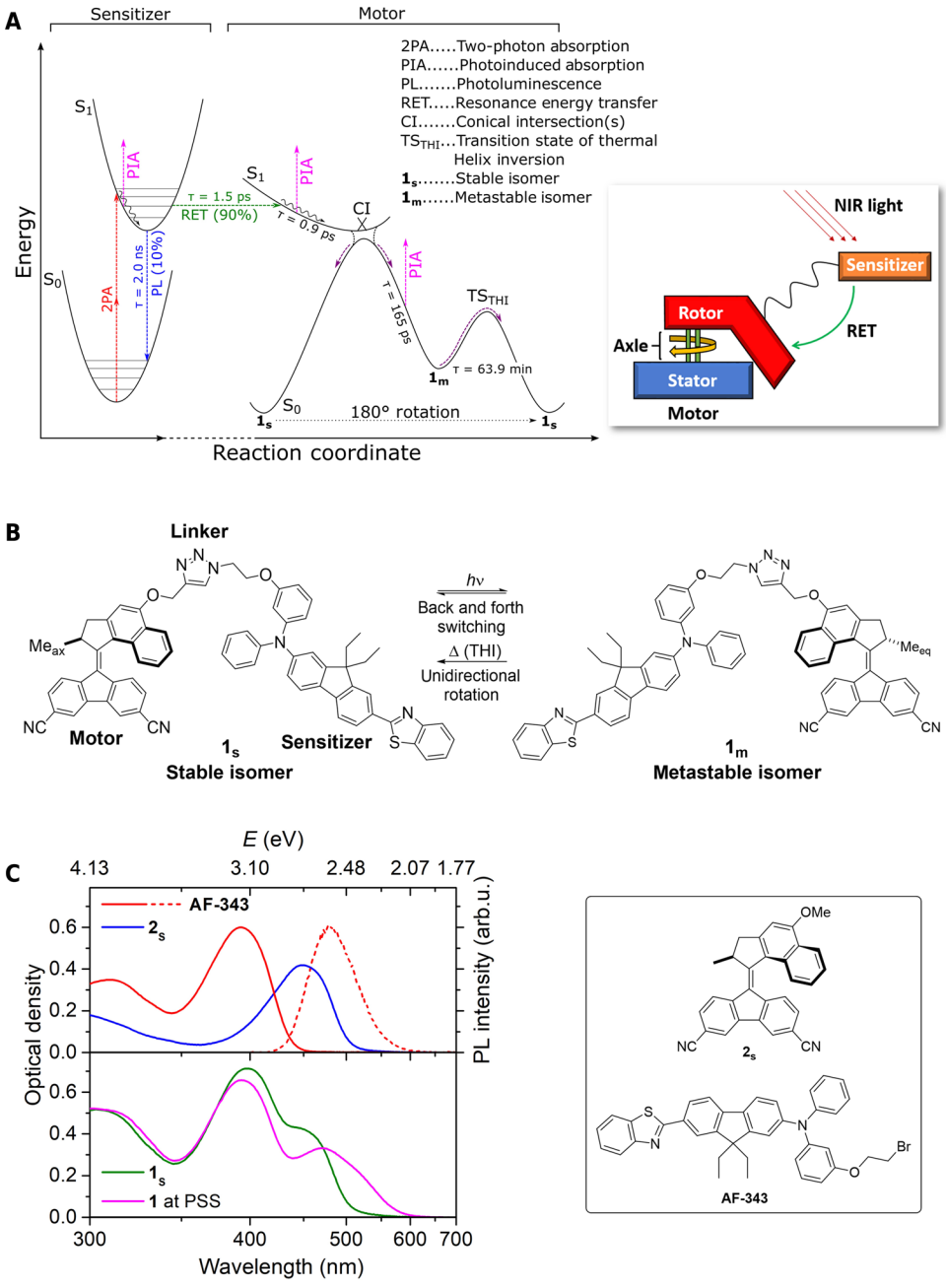

Fig. 1. Concept and design of NIR light–sensitized molecular motor 1. (**A**) Concept, design, and potential energy diagram of NIR light–driven artificial rotary molecular motor. Two photons of NIR light excite a covalently bound sensitizer that transfers the energy to the motor core to initiate rotation. This process can be studied by ultrafast transient absorption (TA) and time-resolved photoluminescence (PL) spectroscopy. The formation of **1$_s$** and **1$_m$** following photoexcitation is expected to pass through two separate CIs as has been shown for a closely related motor (*31*). (**B**) Structure of stable and metastable isomers of motor **1** and their interconversion by light and heat leading to unidirectional rotation. (**C**) Absorption spectra (1.1×10^{-5} M, $CHCl_3$, 20°C) of **2$_s$** (blue), **AF-343** (red), **1$_s$** (green), and the mixture of **1$_s$** and **1$_m$** at the photostationary state (PSS) reached after irradiating **1$_s$** with a 455-nm LED for 5 min (magenta). The dashed curve shows a normalized PL spectrum of **AF-343** using an excitation wavelength of 780 nm. arb.u., arbitrary units.

dynamics were studied in detail by time-resolved transient absorption (TA) spectroscopy.

RESULTS AND DISCUSSION

Figure 1A shows the potential energy diagram describing a 180° rotation of our proposed motor. Energy transfer from the sensitizer following 2PA of incident NIR light promotes the motor domain to its S_1 state, thereby breaking the alkene π-bond to allow free rotation (Fig. 1A). After vibrational cooling of the excited state, the motor passes through a conical intersection (CI) to the ground state forming a mixture of the original stable isomer **1$_s$** and *E*/*Z*-isomerized metastable isomer **1$_m$** as was described earlier (*10*, *29*, *30*). Note that in a study on a closely related molecular motor, Filatov and Olivucci

(*31*) have shown that reactive and nonreactive pathways pass through different CIs. From $\mathbf{1_m}$, the motor progresses to a second, identical stable isomer ($\mathbf{1_s}$) via THI in a unidirectional manner completing a 180° rotation (Fig. 1B). Using this 2PA-RET mechanism of excitation limits the addressable gap between the highest occupied molecular orbital and the lowest unoccupied molecular orbital of the motor domain to $\leq E(S_1)$ of the 2PA sensitizer domain. Therefore, to use incident NIR light, referring to the part of the electromagnetic spectrum between 780 and 2500 nm, this energy difference cannot exceed 3.2 eV. The stable isomer of motor **2** ($\mathbf{2_s}$) with an absorption maximum at 2.7 eV corresponding to $S_0 \rightarrow S_1$ excitation and outstanding photostability is an ideal candidate for our design (*22*). The methoxy group in the rotor half of **2** provides a handle for attaching a 2PA sensitizer without notably altering the electronic properties of the motor. **AF-343** was identified as an excellent choice of 2PA sensitizer due to its large 2PA cross section and the good match of its excited-state energy with that of $\mathbf{2_s}$ (Fig. 1C) (*32*). It was therefore attached to a derivative of **2** to provide motor $\mathbf{1_s}$ in eight linear steps (13% overall yield) from commercial starting materials (for details, see the Supplementary Materials). The UV-vis absorption spectrum of $\mathbf{1_s}$ at >250 nm is the sum of the spectra of the components $\mathbf{2_s}$ and **AF-343** (fig. S11), confirming the presence of two independent π-electron systems at the motor and sensitizer domains, respectively, in line with results from DFT calculations (fig. S4).

Motor function of compound **1** was demonstrated by irradiating a sample of $\mathbf{1_s}$ with 455-nm light. This induces a bathochromic shift of the band centered at 450 nm corresponding to the formation of $\mathbf{1_m}$ (Fig. 1C). After subsequent removal of the light source, the original spectrum and, therefore, $\mathbf{1_s}$ are recovered within 5 hours at 20°C following complete THI (fig. S12). Both processes show a clean isosbestic point at 471 nm, consistent with $\mathbf{1_s}$ and $\mathbf{1_m}$ as the only observable species during rotation (fig. S12), which was confirmed by ^{1}H nuclear magnetic resonance (NMR) (fig. S8). The ratio of $\mathbf{1_m}$:$\mathbf{1_s}$ at the photostationary state (PSS) is similar to **2** upon exclusive direct excitation of the motor domain (table S1). Upon excitation at 395 nm, coinciding with the absorption maximum of the sensitizer unit, a significantly lower PSS was found for compound **1** compared to **2**. This can be explained by taking into account the energy transfer from the sensitizer unit to the metastable isomer of the motor domain leading to photochemical back reaction, providing a first indication that energy transfer from the 2PA sensitizer to the motor unit is taking place. Eyring analysis of the THI of $\mathbf{1_m}$ revealed a standard Gibbs free energy of activation ($\Delta^{\ddagger}G°$) of 91.9 ± 0.1 kJ·mol^{-1}, within error of that of the parent motor (91.7 ± 0.2 kJ·mol^{-1}) (table S2). This is consistent with the limited influence of an increased substituent size on $\Delta^{\ddagger}G°$ observed in earlier studies (*33*). Therefore, upon direct photoexcitation, compound **1** functions as a unidirectional molecular motor analogous to **2**.

To demonstrate the formation of $\mathbf{1_m}$ and subsequent THI following 2PA, steady-state UV-vis absorption spectra of a solution of $\mathbf{1_s}$ in $CHCl_3$ were recorded before and after irradiation with 800-nm, 100-fs pulses; their difference (ΔOD) spectrum is depicted in Fig. 2A (green spectrum). The difference absorption spectrum revealed a distinct bathochromic shift of the absorption band centered at 450 nm, showing a clean isosbestic point at 475 nm following irradiation (Fig. 2A). These observations are identical to those made for direct one-photon excitation with a 455-nm light-emitting diode (LED) (Fig. 1C) and therefore clearly demonstrate the formation of $\mathbf{1_m}$. ΔOD shows a quadratic dependence of the extent of photoswitching on incident light intensity (Fig. 2A, inset), which is fully consistent with the 2PA mechanism. Varying the sample concentration while keeping the intensity constant results in a linear dependence of the amount of $\mathbf{1_m}$ being formed (fig. S19A). This observation supports RET over emission reabsorption as the dominant mechanism of excitation for the motor domain. With through-bond electron exchange interactions decreasing exponentially with distance (*34*) and a minimum distance of nine bonds separating the sensitizer and motor domains, electron exchange interactions (Dexter mechanism) through the linker are not contributing substantially to this energy transfer. The absence of indicative changes in ^{1}H NMR (fig. S10) and the absorption spectra (fig. S11) of the two domains in $\mathbf{1_s}$ compared to separately recorded spectra of $\mathbf{2_s}$ and **AF-343** rule out through-space interactions between the orbitals of their respective π-systems (at least in the ground state), suggesting this pathway of Dexter energy transfer to also not be efficient. Coulombic interactions (Förster-like mechanism) are therefore thought to dominate the mechanism of RET in $\mathbf{1_s}$.

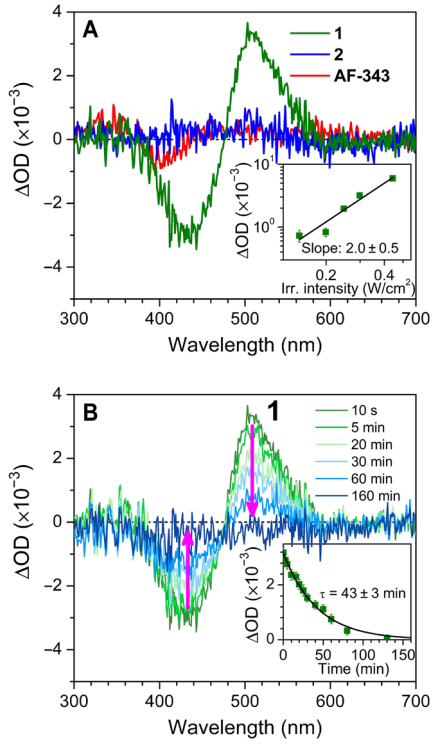

Fig. 2. Comparison of absorption spectra before and after NIR light irradiation. (**A**) Difference absorption spectra (ΔOD) of **1** (green), **2** (blue), and **AF-343** (red) after irradiation at 800 nm for 30 min and keeping the sample in the dark for 10 s. The inset shows the dependence of ΔOD of **1** around 510 nm on the irradiation intensity. The black line shows the fit to a power law function, $y = ax^n$ with n = 2.0 ± 0.5. (**B**) Time evolution of difference absorption spectra of a sample of **1** after irradiation at 800 nm for 30 min and keeping it in the dark between 10 s and 160 min. The magenta arrows depict the thermal recovery of $\mathbf{1_s}$ via THI from $\mathbf{1_m}$. The inset shows the decrease of ΔOD around 510 nm over time together with an exponential fit (black line) with a lifetime, τ, of 43 ± 3 min. In both (A) and (B), the irradiation intensity was 0.3 W/cm^2. ΔOD data for the insets were averaged in the 500- to 520-nm spectral window; the error bars refer to the SD. The molar concentration of all compounds was set as ~1.7 × 10^{-5} M with $CHCl_3$ as the solvent.

Figure 2B shows the recovery dynamics of the original spectrum as time progresses. The full recovery takes ~2.5 hours with the decay following a first-order rate law with a lifetime, τ, of 43 ± 3 min at ambient temperature (~22 ° C). This matches well the lifetime of 49.8 ± 0.4 min calculated from the thermodynamic parameters of activation (table S2). Spectral changes indicative for the formation of $\mathbf{1_m}$ from $\mathbf{1_s}$ could still be observed at peak intensities of irradiation as low as 1.5 GW/cm^2 (corresponding to an average intensity of 0.15 W/cm^2; fig. S17B). This is several decimal orders of magnitude lower than the threshold at which onsets of damage in cells and tissue have been observed (*28*) and which were used for direct two-photon excitation of molecular motors (*27*). The intensity applied is also in line with the 2PA cross section of **AF-343** used herein as the sensitizer (~8100 GM) (*32*) and of unsensitized molecular motors (~9 GM) (*27*).

Irradiating samples of **AF-343** and $\mathbf{2_s}$ under identical conditions did not lead to any observable change of the steady-state absorption spectra, ruling out direct 2PA-induced photoswitching of the motor domain or degradation as causes for the effects observed with $\mathbf{1_s}$ (Fig. 2A). A 1:1 mixture of $\mathbf{2_s}$ and **AF-343** in $CHCl_3$ displayed smaller but otherwise similar spectral changes to $\mathbf{1_s}$ when irradiated with 800-nm, 100-fs pulses (section S6). The spectral response of this mixture was found to decrease quadratically upon diluting the studied solution, leading to a rapid loss of signal. Time-resolved photoluminescence (PL) measurements revealed no difference in the emission behavior of **AF-343** in the presence of $\mathbf{2_s}$, suggesting this effect to be caused by reabsorption of the upconverted light emitted by **AF-343** (see section S8). Compared to the chemically linked system **1**, this mechanism has several drawbacks for applications, especially in vivo. First, the high concentrations of compounds $\mathbf{2_s}$ and **AF-343**, deliberately chosen here to demonstrate the effect, might not be compatible with biofunctionalities and could lead to adverse side effects. Second, by using two separate compounds, one has to solve the problem of colocalization in the relevant parts of the studied organism. Third, under biological conditions, other compounds will compete for reabsorption of the in situ generated PL. Nonetheless, the emission-reabsorption mechanism might open up previously unidentified pathways for systems where chemical attachment of the chromophore to the motor is not feasible or impedes motor functionality [e.g., in the case of large upconverting nanoparticles (*35*)].

Having demonstrated the very functioning of the sensitized motor using two-photon excitation, we applied TA spectroscopy to study the excited-state dynamics preceding the formation of metastable isomer $\mathbf{1_m}$. Figure 3 shows TA transients of samples of $\mathbf{1_s}$ (green), $\mathbf{2_s}$ (blue), and **AF-343** (red) at 620 nm following two-photon excitation at 800 nm.

At this wavelength, only excited-state absorption of the sensitizer domain can be observed (fig. S21). The ingrowing amplitude in the signal of **AF-343** indicates spectral relaxation at short times (up to 5 ps) (fig. S21D) after which the signal decays with an excited-state lifetime of ~1.5 ns. A quadratic dependence of the signal amplitude ΔOD on the excitation intensity (Fig. 3, inset) confirms the two-photon character of the excitation. Attaching **AF-343** to the motor core leads to a substantial shortening of the lifetime (down to ~1.5 ps), indicating population quenching of the excited state of **AF-343** due to energy transfer to the motor core (vide infra). The efficiency of the transfer can be estimated from the share of the 1.5-ps component as ~90% (for details, see the Supplementary Materials).

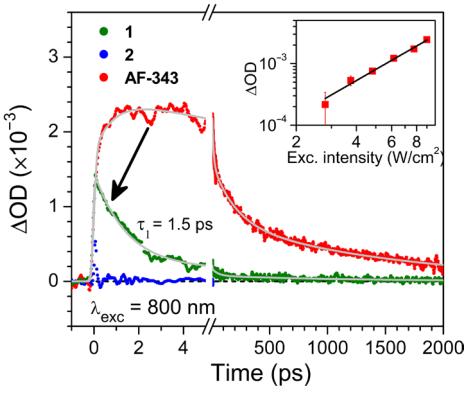

Fig. 3. Excited-state quenching of the sensitizer domain in $\mathbf{1_s}$. TA traces starting from $\mathbf{1_s}$ (green), $\mathbf{2_s}$ (blue), and **AF-343** (red) at 620-nm probe wavelength under two-photon excitation at 800 nm. All transients are solvent-corrected (for details, see the Supplementary Materials). The excitation intensity of all compounds was set as 9 W/cm^2. The gray curves represent fits to multiexponential functions, convoluted with the apparatus function (for the fitting parameters, see table S3). The black arrow indicates excited-state depletion upon attaching the sensitizer to the motor. The inset depicts the ΔOD dependence of **AF-343** on the excitation intensity at a delay of 10 ps. The black line shows the fit to a power law function, $y = ax^n$ with $n = 1.9 \pm 0.1$. The molar concentration of all compounds was set to be similar to ~6×10^{-4} M with $CHCl_3$ as the solvent.

Time-resolved PL measurements confirm all of these conclusions (see section S8).

To study the early-time dynamics of the motor domain in **1**, we recorded TA traces at a 510-nm probe wavelength (i.e., at the point of the strongest response; Fig. 2A) for samples of $\mathbf{1_s}$ and $\mathbf{2_s}$ under two-photon, 800-nm excitation (Fig. 4). No observable signal was detected for $\mathbf{2_s}$, indicating that the bare motor core does not function by direct two-photon excitation. In contrast, the signal detected starting from $\mathbf{1_s}$ is similar to that of $\mathbf{2_s}$ under one-photon excitation (fig. S24). It also shows a quadratic power dependence as expected for two-photon excitation (fig. S25). The TA trace of $\mathbf{1_s}$ decays with a 2.1-ps lifetime, which includes the energy transfer time, i.e., depletion of the **AF-343** excited state with a 1.5-ps lifetime (Fig. 3), and the excited-state lifetime of the motor. The latter can be approximately deconvoluted as 2.1 − 1.5 ps = 0.6 ps, which is reasonably close to the 0.9-ps excited-state lifetime of the motor core (fig. S24A). Alternatively, to extract the early-time signal (<2 ps) related to the motor core alone, we can directly subtract the $\mathbf{1_s}$ and **AF-343** transients (Fig. 4, inset) to obtain a rising time of ~0.9 ps, which is a close match to the 1.5-ps depletion time of the sensitizer excited state. The energy transfer time of 1.5 ps is also in good agreement with that calculated from Förster's relation (see section S9.2). The energy transfer triggers the motor rotation toward the CI at the time scale of 0.6 to 0.9 ps, leading to the formation of $\mathbf{1_m}$. The subsequent structural relaxation of the metastable state is longer than for the bare motor (165 ± 10 ps compared to 16 ± 1 ps; fig. S24A) presumably due to the larger size of **1**. Possible reorientational contribution cannot be ruled out because of identical polarizations used for the pump and probe pulses.

Summary and conclusions

In summary, using our unique design, a multifunctional molecular rotary motor has been realized with the intrinsic ability to operate

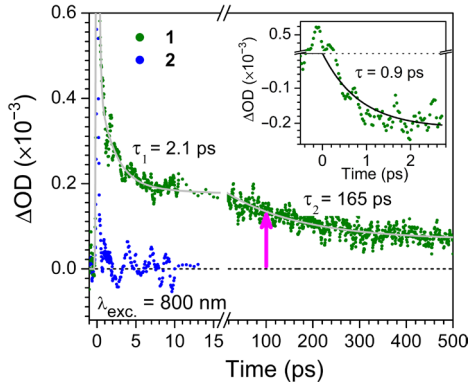

Fig. 4. Ultrafast dynamics of the motor domain in $\mathbf{1}_s$ after RET, leading to formation of $\mathbf{1}_m$. TA traces starting from $\mathbf{1}_s$ (green) and $\mathbf{2}_s$ (blue) at 510-nm probe wavelength under two-photon excitation at 800 nm (9 W/cm^2 excitation intensity). All transients are solvent-corrected (for details, see the Supplementary Materials). The magenta arrow indicates the formation of the photochemically generated metastable isomer $\mathbf{1}_m$. The inset shows the TA transient of **1** at early time with the contribution of **AF-343** subtracted. The black curve is the fit to a function $y = 1 - e^{-\frac{t}{\tau}}$ with τ = 0.9 ps. The gray curve represents the fit to biexponential function (for the fitting parameters, see table S5). The molar concentration of all compounds was set to be similar to ~6×10^{-4} M with $CHCl_3$ as the solvent.

with low-intensity NIR light. Figure 1A presents a summary of the excited-state processes after 2PA by $\mathbf{1}_s$ leading up to the formation of $\mathbf{1}_m$, which subsequently undergoes THI to complete a 180° rotation. The high efficiency of the energy transfer from the dye to the motor domain ensures that the system can operate at NIR light intensities several orders of magnitude lower than the threshold up to which in vivo studies can safely be performed, thereby granting tissue penetration in future applications without risking photodamage. By chemically linking the dye and motor domains, we have ensured that our system remains functional even at very low concentrations and provides an easy solution for the problem of colocalization of motor and sensitizer as required for in vivo applications. Furthermore, using a RET mechanism instead of relying on emission and subsequent reabsorption of upconverted photons minimizes our system's sensitivity to the presence of additional chromophores. The principle of excitation demonstrated here can be applied to any artificial molecular motor with energy levels matching that of the used sensitizer and could, for example, also be expanded to three-photon absorption to use even lower-energy IR light.

By addressing the fundamental challenge of avoiding short-wavelength light, our findings present a gateway to future applications of sensitized molecular motors in biological settings and materials science. Using an upconversion mechanism instead of 2PA for adding up the energies of two or multiple NIR photons may help to further improve the overall efficiency in the future.

MATERIALS AND METHODS

Preparation and characterization of compounds

Reagents were purchased from Sigma-Aldrich, Acros Organics, or TCI Europe and were used as received. Solvents were reagent grade and used without prior water removal unless otherwise indicated. Anhydrous solvents were obtained from an MBraun SPS-800 solvent purification system or directly bought from Acros Organics. Solvents were degassed by purging with N_2 for a minimum of 30 min or by three freeze-pump-thaw cycles.

Flash column chromatography was performed on silica gel (Merck, type 9385, 230 to 400 mesh) or on a Büchi Reveleris purification system using Büchi silica cartridges. Thin-layer chromatography was carried out on aluminum sheets coated with silica gel 60F254 (Merck). Compounds were visualized with a UV lamp and/or by staining with $KMnO_4$, cerium ammonium molybdate (CAM), or vanillin. Motor **2** was prepared as described in the literature (*22*).

^{1}H and ^{13}C NMR spectra were recorded on a Varian Mercury Plus 400 or a Bruker AVANCE 600 NMR spectrometer at 298 K unless otherwise indicated. PSS studies were performed on a Varian Unity Plus 500 NMR spectrometer. Chemical shifts are given in parts per million relative to the residual solvent signal. Multiplets in ^{1}H NMR spectra are designated as follows: s (singlet), d (doublet), t (triplet), q (quartet), p (pentet), m (multiplet), and br (broad). High-resolution mass spectrometry was performed on an LTQ Orbitrap XL spectrometer. Steady-state UV-vis absorption spectra were recorded on an Agilent 8453 UV-vis Diode Array System, equipped with a Quantum Northwest Peltier controller, in 10-mm quartz cuvettes. Irradiation experiments were performed using fiber-coupled LEDs (M420F2, M455F1, M470F3, M490F3, M505F3, and M530F2) obtained from Thorlabs Inc.

Difference absorption measurements

Difference absorption measurements were performed using a UV-vis-NIR spectrometer (Lambda 900) and two different types of light sources for 1PA and 2PA experiments at 455 and 800 nm, respectively. The one-photon irradiation was provided by a fiber-coupled LED (M455F1, Thorlabs) with a maximum output power of 11 mW. The two-photon irradiation was implemented using an amplified mode-locked Ti:sapphire laser (Legend Elite Duo, Coherent) centered at 800 nm with a 1-kHz repetition rate.

TA spectroscopy

TA spectroscopy was performed in a pump-probe arrangement (fig. S1) based on an amplified mode-locked Ti:sapphire laser (Legend Elite Duo, Coherent) centered at 800 nm (1-kHz repetition rate). The laser output was split into pump (~90%) and probe (~10%) beams. For 400-nm excitation, the pump beam frequency was doubled in a β-barium borate (BBO) crystal. A mechanical translation stage (LS-180, Physik Instrumente) with 508-mm excursion was used to delay the probe pulse with respect to the pump pulse. The probe beam was focused into a 2-mm sapphire crystal to generate a white-light (400 to 850 nm) continuum (WLC). A short-pass filter with a cutoff wavelength of 750 nm placed in the probe beam was used to remove residual fundamental frequency radiation from WLC.

Both the pump and the probe beams were focused and spatially overlapped in a 0.2-mm flow cell (Starna Scientific Ltd.), connected to a peristaltic pump (Masterflex, Cole-Parmer) to refresh the sample in the excitation spot. The total volume of the system (including connection tubing and the cell) was ~5 ml. The diameters of the pump and probe beams at the sample position were ~260 and ~170 μm, respectively. The polarization of the pump and probe beams was linear and set to be parallel to each other. The delay of the probe pulse was scanned in 30-fs steps within the 0- to 10-ps range, 0.5-ps steps for the 10- to 100-ps range, and 2-ps steps for the 100- to 2600-ps range.

TA of the probe beam in the flow cell was recorded using two different types of detector, a 500- to 1000-nm compact spectrometer (CCS175/M, Thorlabs) and a silicon photodiode (DET36A, Thorlabs). The spectrometer detected the TA spectra in the range of 500 to 750 nm; however, it had a lower signal-to-noise ratio as compared to the lock-in referenced photodiode.

For spectrometer detection, the pump beam was chopped at 20 Hz by an asynchronous mechanical chopper (Stanford Research Systems Inc.), with the spectrometer locked to the chopper electronics. The differential absorption (ΔOD) of the probe with the pump on and off was calculated for each time delay. Conventionally, negative (ΔOD) signals represent stimulated emission and/or ground-state bleaching, while positive values represent pump-induced excited-state absorption. Last, ΔOD of each pump-probe delay scan was compiled as a function of time and wavelength (for a TA map). This arrangement typically allowed obtaining $\Delta OD \cong 10^{-3}$, which is more than sufficient in the case of one-photon excitation.

For photodiode detection, the pump beam was synchronously chopped at 500 Hz; i.e., every other pump pulse was blocked. The photodetector output was amplified by a lock-in amplifier referenced to the chopper electronics, digitized, and fed to the computer. To obtain the TA signals at a particular probe wavelength (510 and 620 nm), band-pass filters with a full width at half maximum of 10 and 20 nm, respectively, were placed in front of the photodiode. This arrangement improved the sensitivity down to $\Delta OD \cong 4 \times 10^{-5}$, which allowed obtaining the signals under two-photon excitation conditions.

Because of the strong solvent response at early time (<0.5 ps), the TA kinetics under two-photon excitation were corrected by direct subtraction of the separately recorded solvent response (fig. S3). The TA maps and TA kinetics under one-photon excitation were also corrected for the optical density of the sample following the Lambert-Beer law, using the following equation (Eq. 1) (*36*)

$$\{\Delta OD\}_{corr} = \frac{\Delta OD}{1 - 10^{-OD(\lambda = 400\ nm)}} \quad (1)$$

For two-photon excitation, the correction was not needed, and the pump did not experience any direct (one-photon) absorption. As the WLC was not compressed, the time when the pump and probe pulses overlap at a particular probe wavelength was wavelength dependent. For finding the correction curve (i.e., the dependence of the group delay on the wavelength), a TA measurement was performed on chloroform under a sufficiently high peak intensity of >18 GW/cm^2 (corresponding to an experimental average intensity of 1.8 W/cm^2) of the pump pulse, so that a nonresonant TA signal was clearly observed. Then, the transient nonresonant signal was fitted to a combination of a Gaussian—a derivative of the Gaussian function that yielded the zero delay time (*37*). This time was used to determine the zero position of the TA kinetics at 510 and 620 nm.

For spectrometer detection, the transient spectra were extracted from the raw TA map of chloroform by taking spectral slices of 30-fs width at different times (fig. S2A). Each transient spectrum was fitted to a Gaussian function (fig. S2B) to obtain the peak position. The peak positions were fitted to a second-order polynomial function (*38*), yielding the group delay at each particular probe wavelength (gray line in fig. S2A). This function was used to correct the raw TA maps by shifting the data along the time coordinate.

Time-resolved PL spectroscopy

Time-resolved PL spectroscopy was carried out using a Hamamatsu C5680 streak camera equipped with a Ti:sapphire laser (Mira 900, Coherent). To obtain the excitation wavelength of 390 nm, the laser output (wavelength of 780 nm at 76-MHz repetition rate) was doubled in a BBO crystal. For measurements with a time window above 2 ns, the repetition rate was lowered to 2 MHz by a pulse picker. The excitation beam was focused by a 7.6-cm lens into a 1-mm quartz cuvette, containing the studied compounds dissolved in chloroform. The apparatus functions of the setup were ~6 and ~4 ps (SDs of a Gaussian function) for excitation wavelengths of 390 and 780 nm, respectively. The former was measured directly (see section S8.2), while the latter was calculated by squaring the response function of the former.

SUPPLEMENTARY MATERIALS

Supplementary material for this article is available at http://advances.sciencemag.org/cgi/content/full/6/44/eabb6165/DC1

REFERENCES AND NOTES

1. D. Sluysmans, J. F. Stoddart, Growing community of artificial molecular machinists. *Proc. Natl. Acad. Sci. U.S.A.* **115**, 9359–9361 (2018).
2. S. Kassem, T. van Leeuwen, A. S. Lubbe, M. R. Wilson, B. L. Feringa, D. A. Leigh, Artificial molecular motors. *Chem. Soc. Rev.* **46**, 2592–2621 (2017).
3. C. J. Bruns, J. F. Stoddart, *The Nature of the Mechanical Bond: From Molecules to Machines* (John Wiley & Sons Inc., 2016).
4. C. Pezzato, C. Cheng, J. F. Stoddart, R. D. Astumian, Mastering the non-equilibrium assembly and operation of molecular machines. *Chem. Soc. Rev.* **46**, 5491–5507 (2017).
5. W. R. Browne, B. L. Feringa, Making molecular machines work. *Nat. Nanotechnol.* **1**, 25–35 (2006).
6. J. P. Sauvage, P. Gaspard, *From Non-Covalent Assemblies to Molecular Machines* (Wiley-VCH Verlag GmbH & Co. KGaA, 2011).
7. M. Baroncini, S. Silvi, A. Credi, Photo- and redox-driven artificial molecular motors. *Chem. Rev.* **120**, 200–268 (2019).
8. D. Roke, S. J. Wezenberg, B. L. Feringa, Molecular rotary motors: Unidirectional motion around double bonds. *Proc. Natl. Acad. Sci. U.S.A.* **115**, 9423–9431 (2018).
9. B. L. Feringa, The art of building small: From molecular switches to molecular motors. *J. Org. Chem.* **72**, 6635–6652 (2007).
10. J. Conyard, K. Addison, I. A. Heisler, A. Cnossen, W. R. Browne, B. L. Feringa, S. R. Meech, Ultrafast dynamics in the power stroke of a molecular rotary motor. *Nat. Chem.* **4**, 547–551 (2012).
11. R. D. Astumian, How molecular motors work—Insights from the molecular machinist's toolbox: The Nobel prize in Chemistry 2016. *Chem. Sci.* **8**, 840–845 (2017).
12. Q. Li, G. Fuks, E. Moulin, M. Maaloum, M. Rawiso, I. Kulic, J. T. Foy, N. Giuseppone, Macroscopic contraction of a gel induced by the integrated motion of light-driven molecular motors. *Nat. Nanotechnol.* **10**, 161–165 (2015).
13. J. T. Foy, Q. Li, A. Goujon, J.-R. Colard-Itté, G. Fuks, E. Moulin, O. Schiffmann, D. Dattler, D. P. Funeriu, N. Giuseppone, Dual-light control of nanomachines that integrate motor and modulator subunits. *Nat. Nanotechnol.* **12**, 540–545 (2017).
14. J. Chen, F. K.-C. Leung, M. C. A. Stuart, T. Kajitani, T. Fukushima, E. van der Giessen, B. L. Feringa, Artificial muscle-like function from hierarchical supramolecular assembly of photoresponsive molecular motors. *Nat. Chem.* **10**, 132–138 (2018).
15. T. Orlova, F. Lancia, C. Loussert, S. Iamsaard, N. Katsonis, E. Brasselet, Revolving supramolecular chiral structures powered by light in nanomotor-doped liquid crystals. *Nat. Nanotechnol.* **13**, 304–308 (2018).
16. K.-Y. Chen, O. Ivashenko, G. T. Carroll, J. Robertus, J. C. M. Kistemaker, G. London, W. R. Browne, P. Rudolf, B. L. Feringa, Control of surface wettability using tripodal light-activated molecular motors. *J. Am. Chem. Soc.* **136**, 3219–3224 (2014).
17. W. Danowski, T. van Leeuwen, S. Abdolahzadeh, D. Roke, W. R. Browne, S. J. Wezenberg, B. L. Feringa, Unidirectional rotary motion in a metal–organic framework. *Nat. Nanotechnol.* **14**, 488–494 (2019).
18. V. García-López, F. Chen, L. G. Nilewski, G. Duret, A. Aliyan, A. B. Kolomeisky, J. T. Robinson, G. Wang, R. Pal, J. M. Tour, Molecular machines open cell membranes. *Nature* **548**, 567–572 (2017).
19. Q. Zhou, J. Chen, Y. Luan, P. A. Vainikka, S. Thallmair, S. J. Marrink, B. L. Feringa, P. van Rijn, Unidirectional rotating molecular motors dynamically interact with adsorbed proteins to direct the fate of mesenchymal stem cells. *Sci. Adv.* **6**, eaay2756 (2020).

20. S. J. Wezenberg, K.-Y. Chen, B. L. Feringa, Visible-light-driven photoisomerization and increased rotation speed of a molecular motor acting as a ligand in a ruthenium(II) complex. *Angew. Chem. Int. Ed.* **54**, 11457–11461 (2015).
21. T. van Leeuwen, J. Pol, D. Roke, S. J. Wezenberg, B. L. Feringa, Visible-light excitation of a molecular motor with an extended aromatic core. *Org. Lett.* **19**, 1402–1405 (2017).
22. L. Pfeifer, M. Scherübl, M. Fellert, W. Danowski, J. Cheng, J. Pol, B. L. Feringa, Photoefficient 2nd generation molecular motors responsive to visible light. *Chem. Sci.* **10**, 8768–8773 (2019).
23. D. Roke, M. Sen, W. Danowski, S. J. Wezenberg, B. L. Feringa, Visible-light-driven tunable molecular motors based on oxindole. *J. Am. Chem. Soc.* **141**, 7622–7627 (2019).
24. M. Guentner, M. Schildhauer, S. Thumser, P. Mayer, D. Stephenson, P. J. Mayer, H. Dube, Sunlight-powered kHz rotation of a hemithioindigo-based molecular motor. *Nat. Commun.* **6**, 8406 (2015).
25. A. Gerwien, P. Mayer, H. Dube, Green light powered molecular state motor enabling eight-shaped unidirectional rotation. *Nat. Commun.* **10**, 4449 (2019).
26. A. Cnossen, L. Hou, M. M. Pollard, P. V. Wesenhagen, W. R. Browne, B. L. Feringa, Driving unidirectional molecular rotary motors with visible light by intra- and intermolecular energy transfer from palladium porphyrin. *J. Am. Chem. Soc.* **134**, 17613–17619 (2012).
27. D. Liu, V. García-López, R. S. Gunasekera, L. Greer Nilewski, L. B. Alemany, A. Aliyan, T. Jin, G. Wang, J. M. Tour, R. Pal, Near-infrared light activates molecular nanomachines to drill into and kill cells. *ACS Nano* **13**, 6813–6823 (2019).
28. A. Vogel, J. Noack, G. Hüttman, G. Paltauf, Mechanisms of femtosecond laser nanosurgery of cells and tissues. *Appl. Phys. B* **81**, 1015–1047 (2005).
29. J. Conyard, A. Cnossen, W. R. Browne, B. L. Feringa, S. R. Meech, Chemically optimizing operational efficiency of molecular rotary motors. *J. Am. Chem. Soc.* **136**, 9692–9700 (2014).
30. C. R. Hall, J. Conyard, I. A. Heisler, G. Jones, J. Frost, W. R. Browne, B. L. Feringa, S. R. Meech, Ultrafast dynamics in light-driven molecular rotary motors probed by femtosecond stimulated raman spectroscopy. *J. Am. Chem. Soc.* **139**, 7408–7414 (2017).
31. M. Filatov, M. Olivucci, Designing conical intersections for light-driven single molecule rotary motors: From precessional to axial motion. *J. Org. Chem.* **79**, 3587–3600 (2014).
32. R. Kannan, L.-S. Tan, Two-Photon Absorbing Chromophores Containing Polymerizable Olefinic Groups, U.S. Patent 7,067,674 B1 (2006).
33. J. Chen, J. C. M. Kistemaker, J. Robertus, B. L. Feringa, Molecular stirrers in action. *J. Am. Chem. Soc.* **136**, 14924–14932 (2014).
34. M. R. Wasielewski, P. A. Liddell, D. Barrett, T. A. Moore, D. Gust, Ultrafast carotenoid to pheophorbide energy transfer in a biomimetic model for antenna function in photosynthesis. *Nature* **322**, 570–572 (1986).
35. W. Zou, C. Visser, J. A. Maduro, M. S. Pshenichnikov, J. C. Hummelen, Broadband dye-sensitized upconversion of near-infrared light. *Nat. Photonics.* **6**, 560–564 (2012).
36. C. J. Brabec, V. Dyakonov, J. Parisi, N. S. Sariciftci, *Organic Photovoltaics: Concepts and Realization* (Springer, 2003).
37. S. A. Kovalenko, A. L. Dobryakov, J. Ruthmann, N. P. Ernsting, Femtosecond spectroscopy of condensed phases with chirped supercontinuum probing. *Phys. Rev. A* **59**, 2369–2384 (1999).
38. U. Megerle, I. Pugliesi, C. Schriever, C. F. Sailer, E. Riedle, Sub-50 fs broadband absorption spectroscopy with tunable excitation: Putting the analysis of ultrafast molecular dynamics on solid ground. *Appl. Phys. B* **96**, 215–231 (2009).
39. D. Wang, M. V. Ivanov, D. Kokkin, J. Loman, J.-Z. Cai, S. A. Reid, R. Rathore, The role of torsional dynamics on hole and exciton stabilization in π-stacked assemblies: Design of rigid torsionomers of a cofacial bifluorene. *Angew. Chem. Int. Ed.* **57**, 8189–8193 (2018).
40. H. Jiang, J. Sun, Synthesis and characterization of a novel spirocyclic aromatic derivative: Unique roles of phenothiazine. *New J. Chem.* **37**, 3161–3165 (2013).
41. A. Frazer, A. R. Morales, A. W. Woodward, P. Tongwa, T. Timofeeva, K. D. Belfield, Luminescent fluorene-based bis-pyrazolyl aniline ligand for aluminum detection. *J. Fluoresc.* **24**, 239–250 (2014).
42. M. M. Pollard, P. V. Wesenhagen, D. Pijper, B. L. Feringa, On the effect of donor and acceptor substituents on the behaviour of light-driven rotary molecular motors. *Org. Biomol. Chem.* **6**, 1605–1612 (2008).
43. M. Inoue, M. Nakada, Studies into asymmetric catalysis of the Nozaki-Hiyama allenylation. *Angew. Chem. Int. Ed.* **45**, 252–255 (2005).
44. J. Conyard, P. Stacko, J. Chen, S. McDonagh, C. R. Hall, S. P. Laptenok, W. R. Browne, B. L. Feringa, S. R. Meech, Ultrafast excited state dynamics in molecular motors: Coupling of motor length to medium viscosity. *J. Phys. Chem. A* **121**, 2138–2150 (2017).
45. M. J. Frisch, G. W. Trucks, H. B. Schlegel, G. E. Scuseria, M. A. Robb, J. R. Cheeseman, G. Scalmani, V. Barone, G. A. Petersson, H. Nakatsuji, X. Li, M. Caricato, A. V. Marenich, J. Bloino, B. G. Janesko, R. Gomperts, B. Mennucci, H. P. Hratchian, J. V. Ortiz, A. F. Izmaylov, J. L. Sonnenberg, D. Williams-Young, F. Ding, F. Lipparini, F. Egidi, J. Goings, B. Peng, A. Petrone, T. Henderson, D. Ranasinghe, V. G. Zakrzewski, J. Gao, N. Rega, G. Zheng, W. Liang, M. Hada, M. Ehara, K. Toyota, R. Fukuda, J. Hasegawa, M. Ishida, T. Nakajima, Y. Honda, O. Kitao, H. Nakai, T. Vreven, K. Throssell, J. A. Montgomery Jr., J. E. Peralta, F. Ogliaro, M. J. Bearpark, J. J. Heyd, E. N. Brothers, K. N. Kudin, V. N. Staroverov, T. A. Keith, R. Kobayashi, J. Normand, K. Raghavachari, A. P. Rendell, J. C. Burant, S. S. Iyengar, J. Tomasi, M. Cossi, J. M. Millam, M. Klene, C. Adamo, R. Cammi, J. W. Ochterski, R. L. Martin, K. Morokuma, O. Farkas, J. B. Foresman, D. J. Fox, *Gaussian 16, Revision B.01* (Gaussian Inc., 2016).
46. R. Dennington, T. A. Keith, J. M. Millam, *Gauss View, Version 5* (Semichem Inc., 2009).
47. H. J. Kuhn, S. E. Braslavsky, R. Schmidt, Chemical actinometry (IUPAC technical report). *Pure Appl. Chem.* **76**, 2105–2146 (2004).
48. K. Stranius, K. Börjesson, Determining the photoisomerization quantum yield of photoswitchable molecules in solution and in the solid state. *Sci. Rep.* **7**, 41145 (2017).
49. J. Otsuki, K. Suwa, K. K. Sarker, C. Sinha, Photoisomerization and thermal isomerization of arylazoimidazoles. *J. Phys. Chem. A* **111**, 1403–1409 (2007).
50. K. Rurack, M. Spieles, Fluorescence quantum yields of a series of red and near-infrared dyes emitting at 600-1000 nm. *Anal. Chem.* **83**, 1232–1242 (2011).
51. T. Förster, 10th Spiers Memorial Lecture. Transfer mechanisms of electronic excitation. *Discuss. Faraday Soc.* **27**, 7–17 (1959).

Acknowledgments

Funding: We thank the Netherlands Organization for Scientific Research (NWO-CW); the Netherlands Foundation for Fundamental Research on Matter (FOM, a subsidiary of NWO); the Royal Netherlands Academy of Arts and Sciences (KNAW); the European Research Council (Advanced Investigator grant no. 694345 to B.L.F.); the European Commission (MSCA-IF no. 793082 to L.P. and Erasmus+ scholarship to M.S.); the Dutch Ministry of Education, Culture and Science (Gravitation Program 024.001.035); and the University of Groningen for financial support. N.V.H. and M.S.P. have also received funding from the European Union's Horizon 2020 research and innovation program under Marie Skłodowska-Curie grant no. 722651. **Author contributions:** Conceptualization: L.P. and B.L.F. Funding acquisition: L.P., M.S.P., and B.L.F. Investigation: L.P., N.V.H., M.S., and M.S.P. Methodology: L.P., N.V.H., and M.S.P. Resources: M.S.P. and B.L.F. Supervision: M.S.P. and B.L.F. Writing—original draft: L.P., N.V.H., and M.S.P. Writing—review and editing: M.S.P. and B.L.F. **Competing interests:** The authors declare that they have no competing interests. **Data and materials availability:** All data needed to evaluate the conclusions in the paper are present in the paper and/or the Supplementary Materials. Additional data related to this paper may be requested from the authors.

Submitted 6 March 2020
Accepted 14 September 2020
Published 28 October 2020
10.1126/sciadv.abb6165

Citation: L. Pfeifer, N. V. Hoang, M. Scherübl, M. S. Pshenichnikov, B. L. Feringa, Powering rotary molecular motors with low-intensity near-infrared light. *Sci. Adv.* **6**, eabb6165 (2020).